Experimental Techniques (2018) 42:439–452
https://doi.org/10.1007/s40799-018-0247-0

A Practical Procedure for Measuring the Stiffness of Foam like Materials

A.D. Marter[1] · A.S. Dickinson[1] · F. Pierron[2] · M. Browne[1]

Received: 4 August 2017 / Accepted: 28 March 2018 / Published online: 24 May 2018

Abstract

Polymer foams are used extensively in everyday life, from disposable packaging and soft furnishings through to engineering applications such as core structural materials in the marine industry or bone analogue materials for orthopaedic device testing. In the engineering field it is important that the mechanical behaviour of these materials is characterised correctly, as computationally based predictions of structural performance rely heavily on accurate input data. Mechanical property data from standard physical tests such as uniaxial compression are subject to artefacts including non-uniformity of applied loading, test fixture-sample contact conditions, and test machine compliance. These are well-documented problems, which techniques such as extensometry and point tracking of marker pairs attempt to resolve. In particular, in addition to being non-contact, the use of individual marker pairs can reveal non-linear behaviours because of alignment issues. In the current work, a practical, accurate experimental methodology is introduced to investigate this issue. Uniaxial compression tests were conducted on cellular polyurethane foam blocks. Both faces of the foam specimens were monitored using point tracking on multiple marker pairs to account for misalignment. Sample deformation was simultaneously measured by test-machine crosshead displacement. The Young's modulus and Poisson's ratio were calculated in both cases. To verify the measurements, digital volume correlation (DVC) was applied. DVC is a full-field non-contact strain measurement method that interrogates the interior structure of the foam to determine the physical response. Results demonstrated that misalignment effects could easily be followed during testing, which averaged out on both front and back surfaces to produce a single modulus value. Considerable differences were evident between crosshead displacement calculated modulus and point tracking, indicating that artefacts can lead to substantial errors, as evidenced in the published literature.

Keywords Polyurethane foam · Optical extensometry · Point tracking · Digital volume correlation · DVC · Test artefacts · Analogue bone

Introduction

Polymer foams, also referred to as rigid cellular plastics, are used extensively in a diverse range of applications, from domestic furnishings to high-end engineering applications. For the latter, accurate characterisation of the material is essential, particularly for safety-critical applications. To this end, standards have been developed to facilitate mechanical property characterisation. The ASTM standard for measurement of the compressive properties of rigid cellular plastics (D1621) for example, recommends using the test machine crosshead drive system or a direct measurement of compression platen displacement in order to monitor displacement.

In the literature, a number of studies have evaluated the mechanical properties of polyurethane (PU) foams [1–4], primarily in the context of an alternative to trabecular bone, considering compressive [5–8], shear [9] and fatigue [10] properties. However, results have varied markedly as the uniaxial compression test is subject to a number of experimental artefacts that degrade measurement accuracy:

1. Test machine compliance will result in an overestimate of sample deformation if measurement is taken from the test machine crosshead.

Supporting data is openly available from the University of Southampton repository at https://doi.org/10.5258/SOTON/404042.

Electronic supplementary material The online version of this article (https://doi.org/10.1007/s40799-018-0247-0) contains supplementary material, which is available to authorized users.

✉ M. Browne
doctor@soton.ac.uk

[1] Bioengineering Science Research Group, Faculty of Engineering and the Environment, University of Southampton, Southampton, UK

[2] Engineering Materials Research Group, Faculty of Engineering and the Environment, University of Southampton, Southampton, UK

2. Friction occurs between the sample and test machine platens. This may constrain Poisson's effect at the sample ends and cause barrelling of the specimen [11] (Fig. 1a).
3. Misalignment of test machine platens or misshapen sample ends can result in non-uniform loading of the sample (Fig. 1b). This can lead to considerable errors if a single extensometer is used to measure displacement of the sample [12].
4. Finally, localised crushing of the specimen may occur, limiting the strain experienced in the sample bulk (Fig. 1c). Such failure must be identified so that material characterisation is conducted using pre-failure test data only.

The summation of these artefacts generally results in errors in Young's modulus and Poisson's ratio measurements. In particular, point 1) will lead to a systematic overestimation of strain, hence underestimation of Young's modulus. The ASTM standard D1621 does recommend a compliance calibration to correct strain measurements from crosshead displacements, however this correction is often not reported in the literature [1, 6, 7, 9]. For example, a series of studies on a polyurethane foam commonly used as an analogue bone medium, which used crosshead displacement measurements, has reported varying values of Young's modulus for nominally the same foam (Table 1).

There have been attempts to address the mechanical testing issues listed above on foam-like structures. For example, Keaveny et al. [12] have shown that cross-head displacement calculated strains in cancellous bone can lead to substantial errors in Young's modulus (between 20 and 40%). To overcome the problem of platen misalignment, the use of four extensometers was shown to be quite efficient, yet this approach is not adopted in recent publications. More recently, digital image correlation (DIC) techniques have been employed for the assessment of fibre reinforced polyurethane foams [13]. While DIC is data rich and can provide total surface displacement information, its capability is limited when the structure being monitored does not have a pattern that can be tracked easily. For example, a solid foam, a foam with a very small cell size or a foam with a regular pattern would need a random speckle pattern applied on its surface. In addition the accuracy of measurement is driven by the quality of the speckle pattern [14]. In the search for simpler experimental methods that can capture this variability, the objective of the present study was to assess a method of non-contact, direct specimen strain measurement for the characterisation of foam like materials. This was motivated by the need to obtain accurate mechanical property data for computational modelling, and to explain the variability in data reported in the literature. While Keaveny's study investigated the issue of strain measurement in a robust manner, Poisson's ratio was not addressed, and nor was the nominal heterogeneity of stress and strain through the specimen thickness because of the high specimen thicknesses employed in these tests. Extensometers are also subject to several limitations: principally, they may slip on the specimen surface underreading strain, and as they contact the specimen they may influence its behaviour. There may also be practical limitations preventing the measurement of Poisson's effects and accounting for uneven loading, as multiple extensometers would be required across each of a specimen's faces. The present study determines both Poisson's ratio and Young's modulus using an optically based point tracking technique using two cameras, equivalent to Keaveny's four extensometers approach. This is verified using a data rich in-situ X-ray CT/DVC test.

Methodology

Justification of Approach

Non-contact measurement techniques such as i) optical surface extensometry/point-tracking (OT) [15], ii) digital image correlation (DIC) [16–18], and iii) digital volume correlation

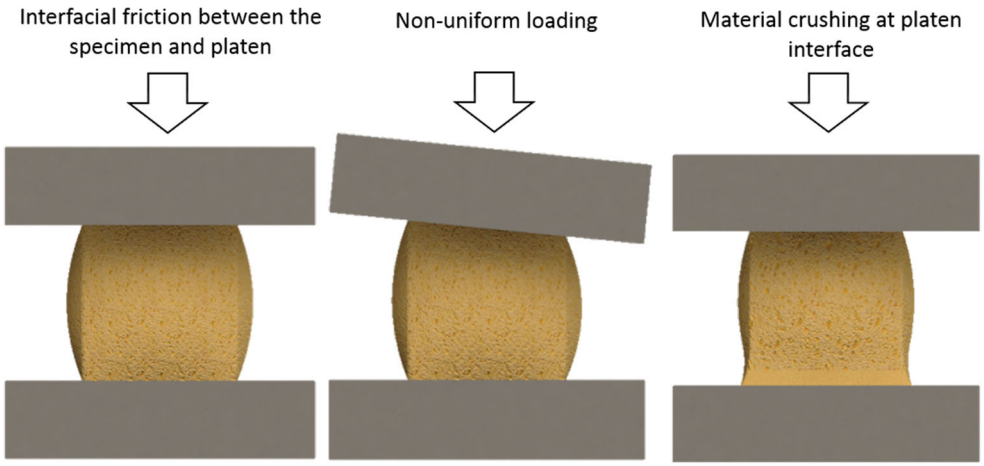

Fig. 1 Sources of experimental errors in uniaxial compression tests. Note: deformations have been exaggerated in order to demonstrate these effects

Table 1 Summary of test parameters and calculated moduli reported in literature and manufacturer technical sheets

Author Measurement method (Foam manufacturer)	Specimen dimensions		Density (kg/m^3)	Loading rate		Young's modulus (MPa mean ± SD)
	length (mm)	Cross-Sectional area (mm^2)		mm/min	Strain rate (s^{-1})	
Sawbones cellular rigid foam [15]	25.4	2580–23,200	320	2.5	1.6×10^{-3}	137
Last-A-Foam [16]	25.4		320	2.5	1.6×10^{-3}	230.2
Szivek et al. 1995 [6] Crosshead displacement (manufactured by author's)	25	625	Not stated	72	48×10^{-3}	110–134
Thompson et al. (2003) [9] Crosshead displacement (Sawbones)	40	314	332 ± 5	1	4.2×10^{-4}	164 ± 27.8 (± 17%)*
Patel et al. (2008) [7] Crosshead displacement (Sawbones)	3.9	64	320 (not measured)	0.78	3.3×10^{-3}	66
	7.9			1.56		145
Calvert et al. (2010) [8] extensometer (Last-A-Foam)	15	45	Not stated	4.5	5×10^{-3}	216 ± 17 (± 8%)*
	25.4	2580	288–352	2.5	1.6×10^{-3}	195 ± 32 (± 16%)*

*plus/minus percentage range from average

(DVC) [19–21] avoid many of the shortcomings associated with contact-based displacement measurement methods. OT uses a structured array of ink point markers on the sample's surface, which are tracked and recorded photographically throughout loading. Image correlation is then used to track the displacement of each individual marker. In a similar manner, DIC measures surface strains by tracking either a naturally occurring or user-generated pattern on the sample's surface. It is the full-field extension of OT where each pixel subset is used as a 'marker'. This requires however, that the specimen be marked by a continuous speckle pattern which is not always easy to achieve, in particular on open cell foams. In the present study, OT is employed as a simpler and less expensive version of DIC. DVC is the bulk extension of DIC where volumes obtained for instance from X-ray computed tomography can be correlated before and after loading if the material exhibits a sufficient natural pattern (i.e., X-ray absorption contrast), which is the case for foams in general [22]. Such non-contact methods remove mechanical extensometer errors (slippage, misalignment), are less sensitive to the test machine end-artefacts listed above [23], and because strain measurements are taken directly on or within the sample, material property assessment should be more accurate as the measurements are not affected by test machine compliance. Use of DVC is advantageous as complete full-field strain measurement is possible and therefore no assumption has to be made that the surface strains represent the bulk strains. While this could be considered as representing the 'gold standard', the test time and cost is significantly higher than camera-based OT.

Sample Preparation

Testing was conducted on cubic samples of 320 kg/cm^3 cellular rigid polyurethane foam (SAWBONES™, Sawbones Europe AS, Malmö, Sweden), all sectioned from the same block using a band saw. Specimens were cut to a nominal edge length of 20 mm to allow sufficient repeating cells (average cell size~1 mm) to satisfy a continuum assumption [24] and maintain suitable CT resolution to resolve cell walls. Four specimens were tested using OT, and the crosshead displacement was also measured for each test. A fifth specimen was tested using DVC. The apparent density of each specimen was calculated by measurement of dimensions by digital callipers and mass by electronic balance (with precisions of 0.01 mm and 0.0001 g respectively) in accordance with ASTM D1622.

Optical Extensometry

The front and back of each specimen were marked with nine dots using a felt-tip pen (Fig. 2) from which discrete tracking pairs were selected. The dot size was approximately 1.5 mm (150 and 100 pixels for the front and back respectively; see Fig. 2 caption). Two cameras (AVT Manta G504B, 2452 × 2056 pixels, 8-bit) fitted with a fixed focal length lens (Sigma 105 mm f/2.8 EX DG Macro) were used to image the specimen's front and back faces (see Fig. 2).

Each specimen was compressed in a screw-driven electromechanical testing machine with a 2 kN capacity load cell (Instron 5569, Instron, High Wycombe, UK) at a displacement rate of 0.15 mm/min (1.25×10^{-4} s^{-1}) from an initial preload of 10 N. To evaluate whether loading rate would influence the results, a second test at 2.5 mm/min (1.6×10^{-3} s^{-1}) was performed. In each test compressive displacement was applied up to a load of 900 N (about 2 MPa). This load was chosen such that the sample remained considerably below the manufacturer-quoted yield strength of 5.4 MPa and behaved elastically. No lubrication was applied to sample-platen interfaces as the transversely constrained boundary

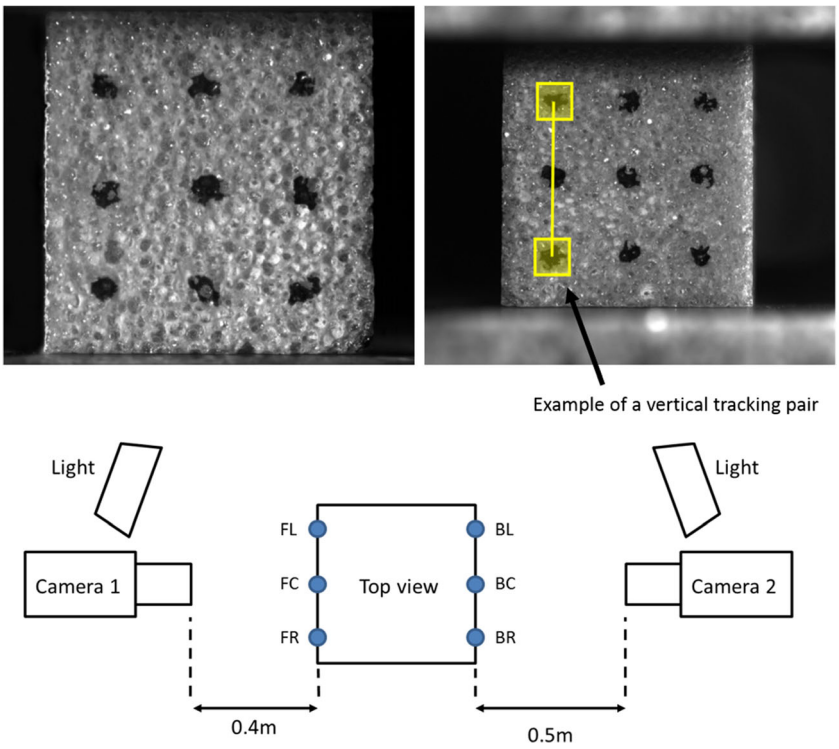

Fig. 2 Marker arrangement and experimental schematic for OT. Note: camera two is further away as the test machine base extended backwards obstructing placement of the tripod. FL: front left; FC: front centre; FR: front right; BL: back left; BC: back centre; BR: back right

condition (due to friction) could be more simply modelled when calculating a surface strain correction factor. During compression, an average of 10 and 75 images were recorded throughout the test for loading rates of 2.5 mm/min and 0.15 mm/min, respectively, with an image exposure time of 500 microseconds. Marker movement was tracked and the displacement of the centre of gravity of each point was obtained by image correlation using the point tracking module of MatchID (www.matchidmbc.com). The uncertainty of the displacement (standard deviation of displacements of all the points between two stationary images) was 0.05 pixels. From this, the strain uncertainty was $0.05/h = 5.6 \times 10^{-5}$, where $h = 900$ pixels was the distance between the dots. An overview of the OT procedure is presented in Fig. 3.

During each test, crosshead displacement was also recorded to allow comparative elastic modulus calculation with the assumption of zero machine compliance. For each measurement technique the modulus was defined by the slope of the linear region of the stress-strain response [6, 8].

Finite Element Analysis Corrections

The applied test conditions and variations in specimen geometry resulted in non-uniform nominal stress and strain states in the specimens. As OT is a surface measurement, the through-thickness variation of axial (z) strain is not accounted for. Strain also varies across the outer surface due to the constraint at the platen interface causing a barrel-like deformation.

To correct for the variations in the specimen geometry and assess variation for different specimen aspect ratios (height, a:width, b), a series of finite element (FE) models were developed within ANSYS v17 APDL (ANSYS Inc., PA USA). Rectangular cuboid models with aspect ratios ranging from 1/3 to 3 (Table 2 and Fig. 4) were constructed from linear isotropic hexahedral elements. The model with an aspect ratio of 1 had a side length of 20 mm, corresponding with the nominal dimensions of the tested specimens. Poisson's ratios ranging between 0.1 and 0.4 were assigned to each geometry configuration to assess surface strain variation. A Young's modulus of 314 MPa was assigned to match modulus identified by the virtual fields method performed on DVC data (detailed below). A single modulus was used as the linear analysis results in a constant ratio of surface and internal strain. Two opposite surfaces were then constrained in the non-loading directions, to simulate the blocked boundary resulting from infinite specimen-platen friction. This may overestimate the effect as some sliding at the interface could occur but it is believed to be much closer to real conditions than free movement. One of these surfaces was then constrained in the z direction and a displacement applied to the other such that a load of 900 N was applied to the specimen.

Surface nodes were then selected corresponding to experimental marker locations. Poisson's ratio and Young's modulus values were then calculated based upon the local displacement of these nodes and the nominal specimen stress, and compared

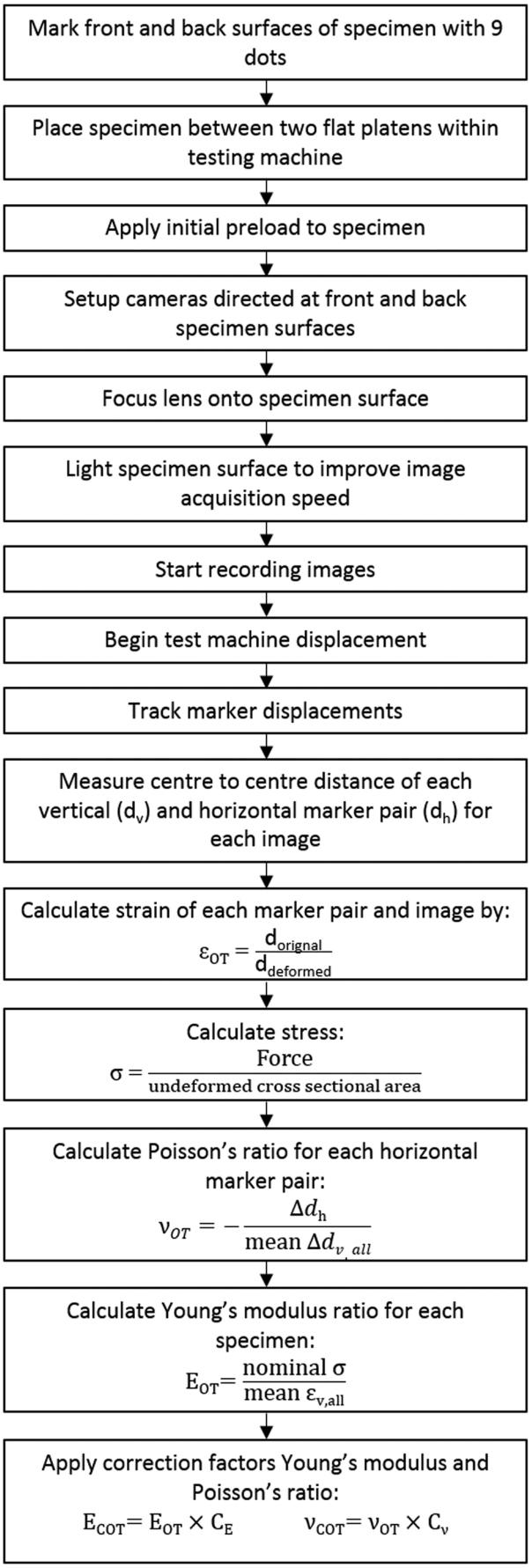

◀ **Fig. 3** Flow diagram of OT procedure, mechanical property calculation and application of FE corrections. ε_{OT} = vertical or horizontal marker pair strain, d = distance between vertical or horizontal tracking pair marker centres, σ = specimen stress, ν_{OT} = horizontal marker pair Poisson's ratio, E_{OT} = specimen Young's modulus, E_{COT} = corrected specimen Young's modulus, ν_{COT} = corrected horizontal marker pair Poisson's ratio

to the model input material properties to provide a correction factor (see Equation (1)).

$$C_\vartheta = \frac{\nu_i}{\nu_o} \quad C_E = \frac{E_i}{E_o} \tag{1}$$

where C_ν and C_E are the Poisson's ratio and Young's modulus correction factors, ν_i and E_i are values input to the model, and ν_o and E_o are the calculated 'output' values. For comparison, DVC correction factors were also derived using the uniaxial strain approach and the VFM from the same computational data, but using deformations in the volume.

Digital Volume Correlation and the Virtual Fields Method

To verify the findings of the optical extensometry technique, a compression test was carried out on a foam block of the same specification and size as the OT specimens'and strain measurements made using the digital volume correlation (DVC) technique in combination with the virtual fields method (VFM).

Micro-focus X-ray computed tomography measurements were performed with a custom 225/450 keV HUTCH μCT scanner, (Nikon/Metris, Tring, UK; muVIS centre, Southampton, UK). A voxel resolution of 17.4 μm was selected such that the specimen filled the field of view and pore walls could be visualised (Fig. 5). Each scan consisted of 2502 projections, with 4 frames per projection to improve the signal to noise ratio. An X-ray tube potential of 100 kV and power of 75 μA enabled sufficient contrast and penetration of the specimen. Image reconstruction to a 32 bit 2000 × 2000 × 2000 volume was performed using CT-Pro (Nikon, Tring, UK). Volumes were down-sampled to 8 bit and cropped to a 1200 × 1200 × 1100 volume with only the foam, to reduce data processing time. It has been shown by Gillard et al. [11] that these operations does not degrade the quality of the DVC results.

Table 2 Summary element and node number for each aspect ratio modelled

Model aspect ratio	1	2	3	1/2	1/3
Element number	219,600	439,200	338,700	871,200	1,009,200
Node number	230,700	457,600	355,300	900,500	1,044,400

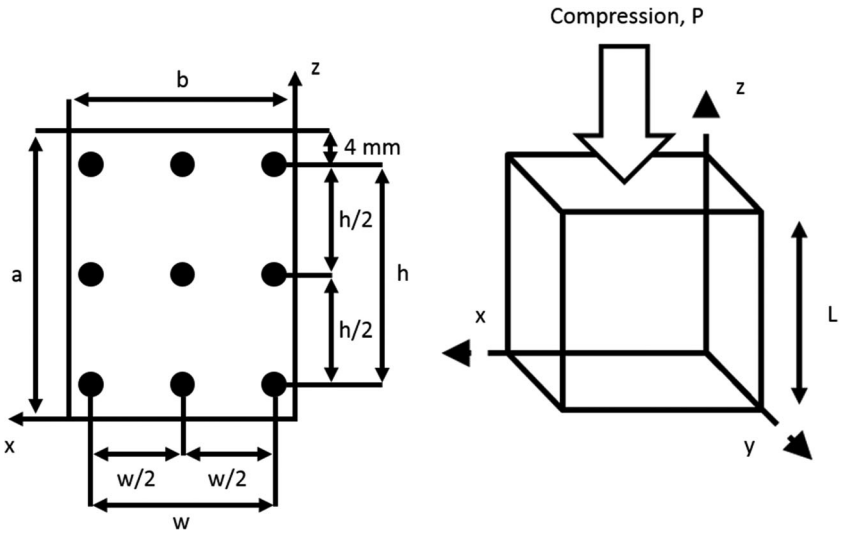

Fig. 4 Left) aspect ratio configuration. Right) coordinates and loading conditions

The specimen was placed between two PVC end platens of an *in situ* loading rig (Deben UK Ltd., UK). Following best practice reported in the literature [11], an initial series of repeat scans were first performed to quantify background noise and determine adequate DVC parameters (Table 3). The strain behaviour was then characterised by applying axial displacement in 0.1 mm increments for eight load steps with scans between each. The desired displacement of each step was applied at a rate of 1 mm/min with load measured throughout the duration of the test. Each scan was conducted following a 20-min wait to allow for load stabilisation.

DVC analysis was performed using DaVis software (Lavision, Göttingen, Germany). Analysis was first performed on repeat scans in the absence of loading, to assess the effect of systematic background noise. A subvolume size of 96 voxels and overlap of 50% were found to give an appropriate compromise between noise reduction and spatial resolution for the imaged material (Fig. 5). Strains were calculated by centred finite differences without additional smoothing. A direct Zero-mean Normalized Cross Correlation (ZNCC) criterion was used to account for any bulk greyscale changes or offset between scans. Third order spline interpolation was used to improve the accuracy of sub-voxel displacement measurement.

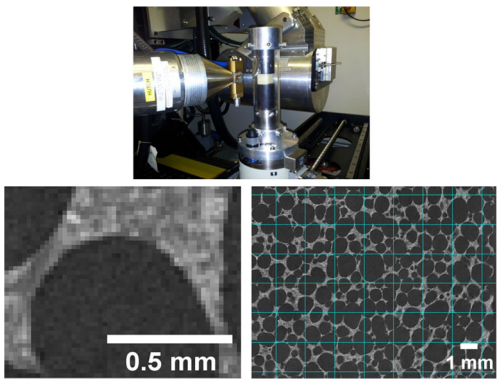

Fig. 5 μCT Scanner and *in situ* loading rig containing cubic specimen (top); resulting example CT section (bottom left and right). Bottom right includes subvolume sized (96 voxel) grid

The virtual fields method (VFM) was used to remove the effect of possible uneven loading in the calculation of Young's modulus and Poisson's ratio. The VFM has been successfully used to investigate the mechanical properties of a variety of materials, including composites [25, 26], polymers [27, 28], and metals [29, 30]. These studies used surface measurements, requiring the assumption of through-thickness uniformity. Gillard et al. [11] used full-field micro CT data with DVC analysis to determine the Poisson's ratio of porcine cancellous bone. However, their experimental setup did not allow for *in situ* measurement of load and hence Young's modulus was not obtained.

The VFM uses full field strain data to find a stress field that satisfies equilibrium. This is based on the principle of virtual work, which is the work done on a particle by the forces which act on it following the application of a hypothetical displacement [31]. Once the stress field is known, and displacement is monitored by following identifiable features within the material volume, it is possible to determine Young's modulus and Poisson's ratio of the material. For a full description of the VFM, the reader is referred to the work of Pierron and Grédiac [32].

For verification, Poisson's ratio and Young's modulus were also calculated by using the spatial averages of ε_{xx}, ε_{yy} and ε_{zz} over the entire volume and the σ_{zz} stress from the compressive load divided by the loaded cross sectional area. This however assumes a uniaxial state of uniform compressive stress, while the VFM does not.

Results

Test machine compliance, platen/specimen friction, misalignment and crushing of the specimen can affect the measurement

Table 3 Summary of DVC parameters and repeat scan noise

DVC parameters				
Subvolume size (voxel)	Overlap (%)	Correlation criterion	Interpolation	Shape function
96	50	ZNCC	3rd order spline	Linear
Repeat scans				
Standard deviation of strain	Standard deviation of displacement (voxel)	Mean strain	Grey level noise (% dynamic range)	
1.4×10^{-4}	0.008	1.22×10^{-5}	0.3	

of strain. The issue of crushing was circumvented in this study by operating well below the yield strength of the material. However, the remaining factors could have influenced strain measurement and are each presented below.

Test Machine Compliance

Modulus calculated by crosshead data was 172 MPa and 174 MPa for specimens tested at 2.5 mm/min and 0.15 mm/min (Table 4), respectively. However, these results include the deflection of the test machine, leading to an underestimation of Young's modulus of the specimen. By using the OT technique, calculated from the average of the six strain measurements, then scaled by the FE derived correction factor to account for through thickness strain variation, specimen displacements are directly measured and hence exclude machine compliance effects. This led to the average elastic modulus derived from the OT data of 321 MPa and 349 MPa for specimens tested at 2.5 mm/min and 0.15 mm/min (Table 4), respectively.

Platen Misalignment

Using the OT technique, it is possible to track how strain varies in a specimen as a result of platen misalignment

Table 4 Summary of sample dimensions, loading parameters and elastic modulus results

Method	Sample dimensions		Density (kg/m^3)	Loading rate		Young's modulus MPa mean (range)
	height(mm)	Cross-Sectional area (mm^2)		mm/min	Strain rate (s^{-1})	
OT (uncorrected)	20	400	323 ±2.60	2.5	2.1×10^{-3}	358 (306-411)
				0.15	1.25×10^{-4}	390 (340-436)
OT (corrected[a])				2.5	2.1×10^{-3}	321 (276-370)
				0.15	1.25×10^{-4}	349 (305-390)
Crosshead displacement				2.5	2.1×10^{-3}	172 (165-183)
				0.15	1.25×10^{-4}	174 (173-189)
DVC (constant stress)			314	Quasi static		331
DVC (constant stress corrected[a])						307
DVC (VFM)						314

[a] adjusted by strain inhomogeneity correction factor (see discussion). Only green cells provide accurate modulus values (relative to 'gold standard' VFM/DVC)

(illustrated in Fig. 1). For example, tracking the movement of the FL and BL markers (Fig. 2) allows the stress-strain response on the left of the specimen to be determined. In one specimen (Fig. 6a), the response is initially non-linear, with a rapid stress increase followed by a linear region. Conversely, the stress-strain curve for marker pairs FR and BR produced an almost mirrored response, with a marked toe-in before becoming linear, indicating that while load is applied immediately on the left of the specimen, there is a delay before the load is registered on the right hand side. By averaging each vertical tracking pair front to back any non-uniform loading in this direction was removed, as well as possible effects of out-of-plane movement. This resulted in the central region response converging towards the linear all-marker average (Fig. 7a). As some non-uniform loading still occurred left to right, the front-to-back averaged marker pairs on the outer extremity still showed a non-linear response, mirroring the response of the other side. A similar effect was noted in a further specimen where uneven loading primarily propagated from front to back (Figs. 6b and 7b). When measurements were averaged across all locations a near linear response was observed ($R^2 > 0.99$). For each specimen, the maximum strain observed varied by measurement location, typically between 2000 με and 7000 με. This resulted in a maximum variation in Young's modulus of 80 MPa (front to back) and 73 MPa (left to right), representing 19% and 17% of the mean response across the whole specimen.

Platen-Specimen Friction

The FE results showed that platen-specimen constraint resulted in increased compressive z strain at the specimen's centre compared to the surface. The x and y strain distribution showed regions of diminished strain extending in the z direction from the blocked boundary condition (Fig. 8). This strain distribution is evident from the response of the transverse marker pairs (Fig. 9). Poisson's ratio was calculated from the top, centre and bottom specimen marker pairs on both the front and back of each specimen. In each case Poisson's ratio was derived by the average strain of all six vertical marker pairs. In all specimens the central section expanded the most giving the largest Poisson's ratio of 0.33. As expected due to the constraint provided by the non-lubricated platen to specimen contact, Poisson's ratio calculated at the top and base was lower, averaging to 0.26. Following the application of the FE correction factors Poisson's ratio became 0.30 at the centre and 0.34 near the specimen-platen interface. A summary of all calculated Poisson's ratio values is provided in appendix Table 7.

The influence of platen constraint could be observed in particular by varying the specimen dimensions. When calculated by surface strain points (the OT markers) and averaged uniaxial stress/strain, FE results showed that altering the specimen aspect ratio and input Poisson's ratio had a considerable effect on calculated Young's modulus and Poisson's ratio. Accuracy was lowest for the OT and averaged uniaxial stress/strain approaches when lower aspect ratios were modelled. However, calculated material properties tended to the modelled values for aspect ratios greater than 1. For both of these methods, error in the calculated Poisson's ratio was greater for smaller input Poisson's ratios. The opposite trends were observed for calculated Young's modulus. For the benefit of other researchers, the correction factors are presented for application to experimental data after applying a second order polynomial to the data extracted from the FEA models (appendix Tables 5 and 6). Little variation was observed between input material properties and those calculated by the virtual fields method (difference < 1%).

DVC Verification

The Young's modulus of the foam derived from DVC data was 331 MPa and 314 MPa when calculated from the uniaxial stress approach and VFM, respectively (Table 4). Poisson's ratio results from DVC data were 0.35 and 0.33 when calculated from the uniaxial stress approach and VFM, respectively (appendix Table 7).

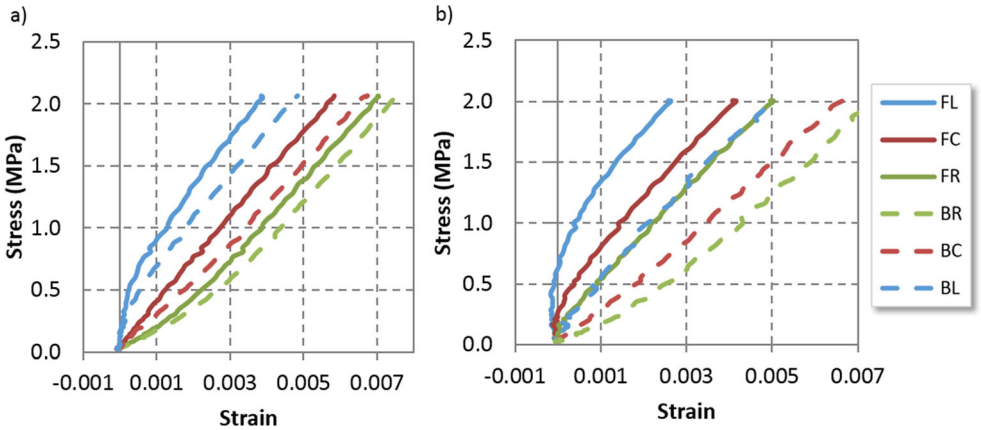

Fig. 6 OT loading response split by vertical marker pairs showing dominant (**a**) left to right, and (**b**) front to back uneven loading. Note: Stresses and strains here are represented within positive quadrant although compressive loading was applied to the specimen

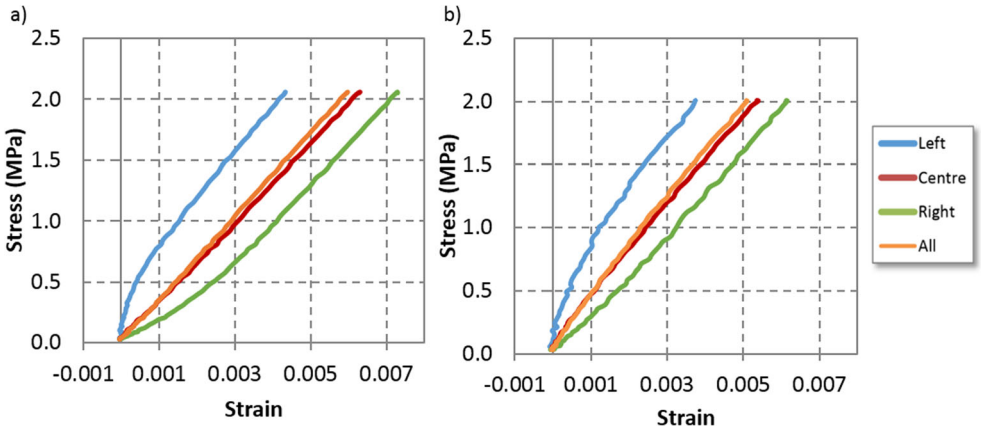

Fig. 7 OT loading responses split by vertical marker pairs averaged front to back. Note: stresses and strains here are represented within positive quadrant although compressive loading was applied to the specimen

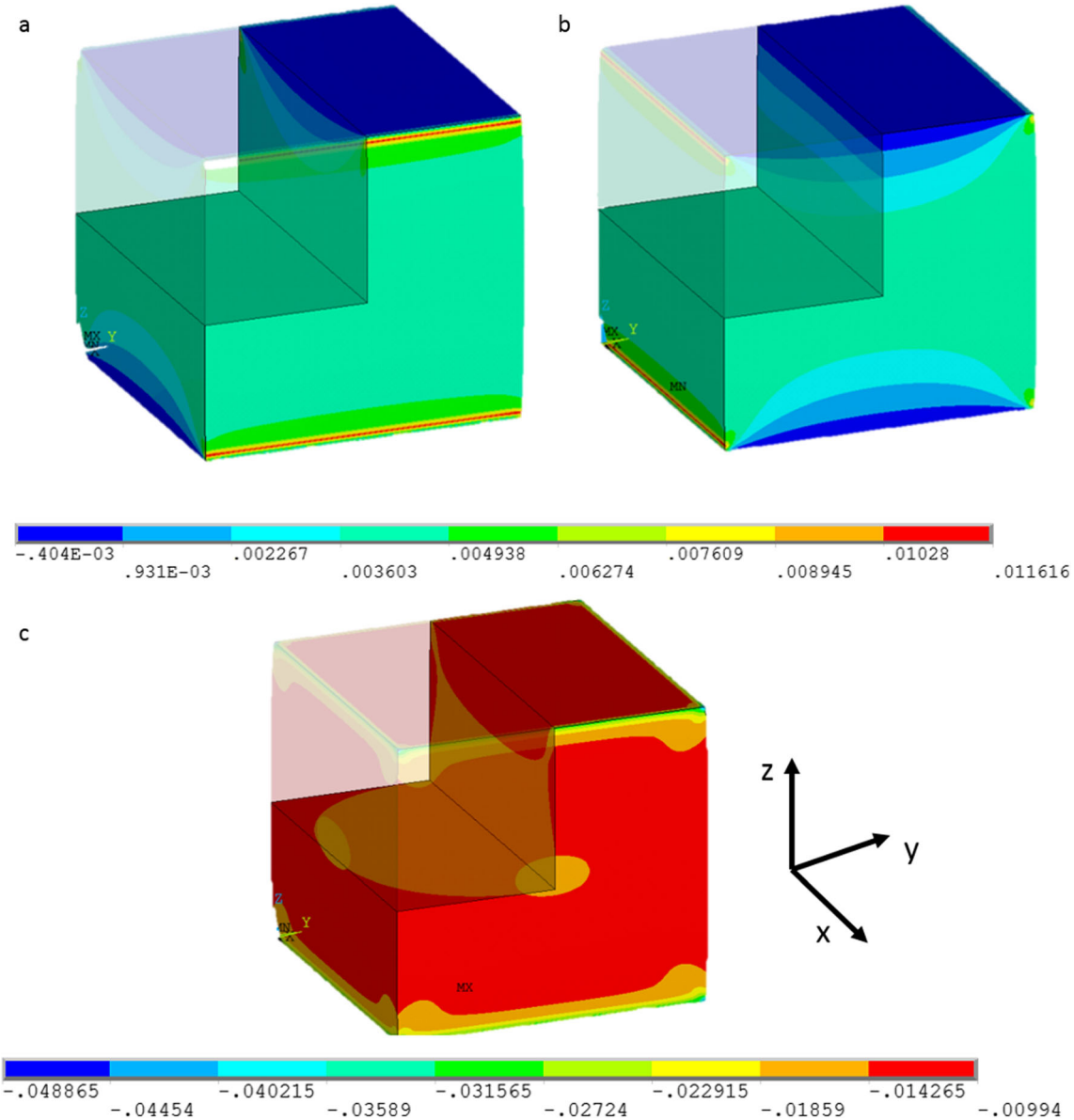

Fig. 8 Strain profiles calculated by FEA. (**a**) x-strain, (**b**) y-strain, (**c**) z-strain

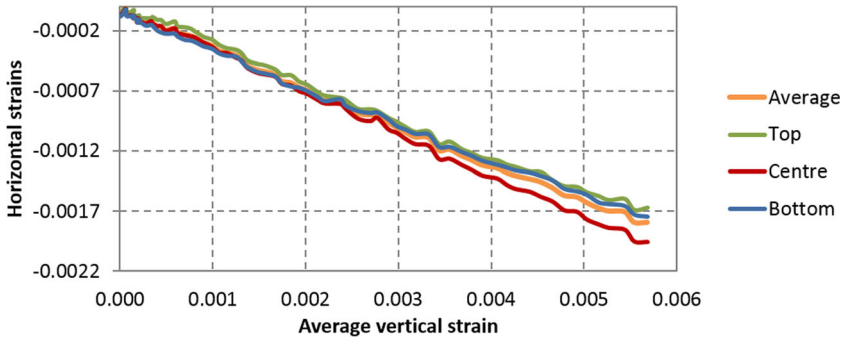

Fig. 9 Horizontal strains at each marker pair height against averaged vertical strain. Note: Strains here are represented within positive quadrant although compressive loading was applied to the specimen

Testing more specimens would enable an estimation of material variability but this is beyond the scope of the present methodology paper. Significantly, the results show that crosshead displacement based measurement would underestimate the modulus by a factor two, whereas both OT with front-back / side-to-side averaging, and DVC provide consistent values. The averaged stress-strain behaviour calculated by each of the three experimental methods is plotted in Fig. 10.

Discussion

The properties of polymer foams can vary widely depending on factors such as the material, its structure (open cell or closed cell), density, the orientation of the cells, and the strain rate at which it is tested. It is important that their mechanical properties are characterised accurately, as this supports the design process, where computational modelling based on measured mechanical properties is often used, particularly for engineering polymers in safety critical applications.

The need to understand the effects of test artefacts is clearly demonstrated in the work of Patel et al. [7], who measured deformation from crosshead displacement during compression testing of cylindrical polyurethane foam specimens of lengths (L) 3.9 and 7.7 mm. It was found that the Young's modulus of the short specimen (66 MPa) was less than half that of the long specimen (145 MPa), and this was attributed to the influence of specimen geometry. However, machine compliance could explain this difference. The measured strain from the crosshead displacement contains contributions from the test machine compliance (d_m/L) and the specimen (d_s/L). The machine compliance effect should be the same for both specimens as their axial stiffness is the same. Therefore, for a smaller specimen, the proportion of the overall strain arising from the machine's deformation (d_m) will be larger, giving an artificially lower Young's modulus value.

In the present study, the average Young's modulus derived from OT was 94% higher than that using crosshead measurements, and 144% higher than manufacturer provided values (Fig. 11). However, the difference between optical and crosshead displacement-derived values were similar to that reported by Keaveny et al. [12] where four extensometers were placed around the specimen to account for errors in misalignment. The method used in the present study has the additional advantage of transverse measurement enabling the calculation

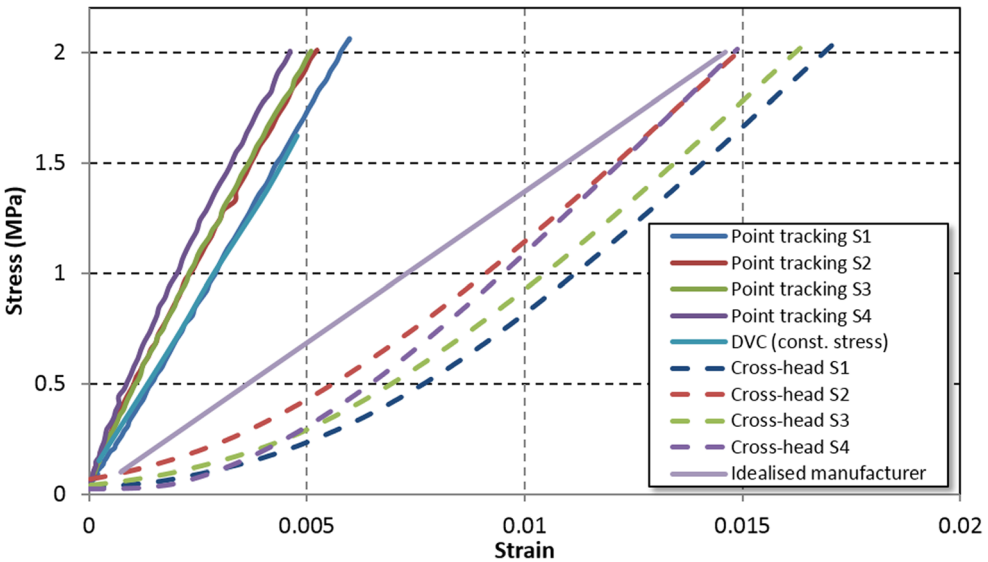

Fig. 10 Stress-strain curve for each measurement method. Correction factors have been applied to non-contact methods. For comparison, an idealised stress-strain plot for the manufacturer-quoted modulus is shown. Note: Stresses and strains here are represented within positive quadrant although compressive loading was applied to the specimen

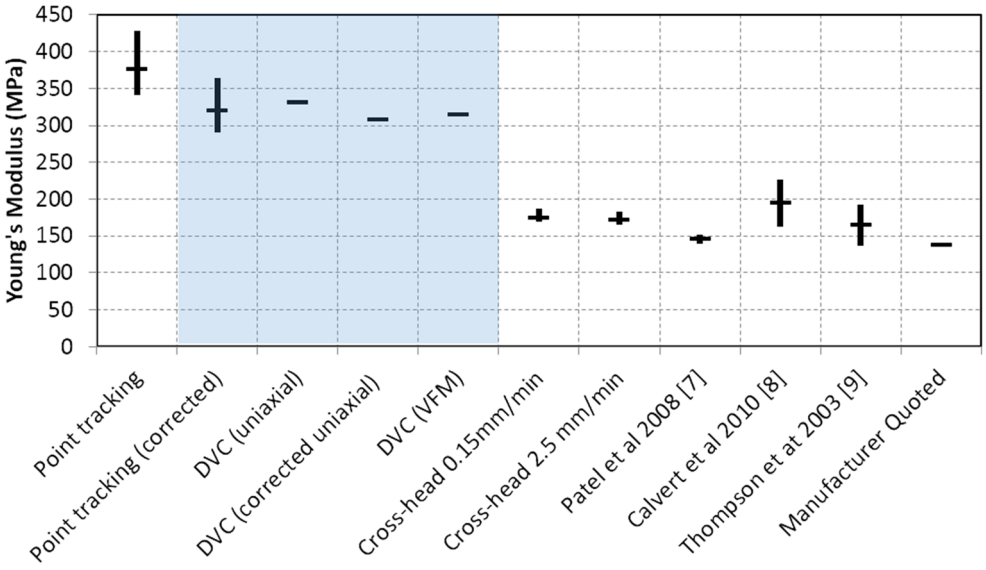

Fig. 11 Comparison of calculated Young's modulus across different measurement methods and previous studies. Markers show mean and range of calculated/ reported Young's modulus

of Poisson's ratio. Such a high discrepancy in Young's modulus could have implications for modelling the foam, where, for example, the assignment of a lower Young's modulus for the foam (often used to represent bone) based on manufacturer quoted values, would predict higher than expected deflection of an implant under loading. A further advantage of the OT method is the avoidance of test machine dependency, through direct measurement of the sample itself. Testing the same material on two different machines could lead to different stress/ strain responses, which in turn would lead to variances in Young's modulus (Table 1 and Fig 10).

Using OT, the average Young's modulus was 374 MPa, 13% higher than the DVC results (Table 4 and Fig. 11). However, on inspection of the FE data for this specimen geometry, the average z-strains over the specimen volume were 10.5% higher than those at the surface. Using this as a correction factor the estimated elastic modulus becomes 335 MPa, within 6% of the reference DVC calculated modulus, where strains are measured and averaged in the volume, inherently accounting for this inhomogeneity.

One of the difficulties when using single camera imaging for OT or DIC is that any out-of-plane movement will result in spurious strains by changing the magnification [33]. The out-of-plane movements caused by Poisson's effect can be neglected [28] but any rigid-body movement will generally cause significant strains. These spurious strains are given by dx/x where dx is the out-of-plane movement and x is the imaging distance. However, if the specimen moves forward to the front camera, causing a positive spurious strain, it will move away from the back camera, causing a negative strain of the same magnitude. Hence, averaging between front and back using two cameras effectively removes this effect, as demonstrated in Moulart et al. [34]. Using this configuration, any misalignment or uneven loading that occurs may also be compensated by averaging across tracking pairs (Moulart et al. [34]). Use of horizontal marker pairs enabled Poisson's ratio calculation at different heights of the specimen. This configuration is equivalent to the four extensometers approach of Keaveny et al. [12], where the side markers replace markers on the lateral faces, enabling the use of only two cameras instead of four, which greatly simplifies the procedure.

OT strain results showed notable variability at different measurement locations on the same specimen (Fig. 6), indicating non-uniform loading did occur within all specimens, despite the care taken to try to apply uniform loading. However, averaging across multiple points compensated for these effects, as also reported in Keaveny et al. [12], and yielded linear profiles. This approach has also been adopted in plate specimens, where front and back strains differed substantially but averaged to give the expected result [34–36]. The observed variability is likely multi-causal (specimen shape, platen-specimen contact, platen to test machine connection, test machine crosshead alignment, out-of-plane specimen movement), highlighting the need to measure at multiple locations, the importance of avoiding specimen skew during preparation, and the large errors resulting from crosshead displacement use. When all experimental care described previously has been taken, intra-specimen variability was low in comparison to inter specimen variability. As the foaming rise direction was not recorded prior to the machining of specimens, and specimens were always tested in the same direction, it is possible that material anisotropy caused some of the inter-specimen variability. In addition, the sample material included short fibre reinforcement of unknown fibre orientation and distribution. As such the sample dimensions may not have been sufficient to ensure completely uniform properties between specimens.

The FE results illustrate that the VFM, which used bulk measurements, was completely insensitive to specimen aspect

ratio as there is no hypothesis on stress state and volume strains are processed instead of surface strains. For the OT approach it was evident that testing samples with aspect ratios less than one should be avoided, as this could result large errors to both Young's modulus and Poisson's ratio, unless correction factors were applied.

The Poisson's ratio measurements were consistently higher at the centre of the specimen face. As the Poisson's ratio is unlikely to vary so much within one sample, this confirms that the loaded surfaces were constrained by frictional effects at the test machine platens resulting in reduced transverse deformation at the sample ends. Once averaged front-to-back, Poisson's ratios measured at the top and bottom typically converged to within 10%. This may be explained by marker position variability. After the application of the correction factor Poisson's ratios from each location did not converge to a single value indicating that the fully transverse displacement constrained boundary condition overestimated the constraint as some sliding must occur at the specimen/platen interface. In practice, this means that the correction factors in appendix Tables 5 and 6 are overestimated for the areas close to the specimen's top and bottom boundaries, which is consistent with the corrected results in Table 7 (after correction, Poisson's ratios at the top and bottom are slightly larger). Following the application of the correction factor the average Poisson's ratio was 0.33, within 3% of that calculated by DVC.

The Young's modulus values derived from crosshead displacement were 27% higher than manufacturer quoted values, but consistent with the range of values found in literature for the same density foam [9]. Modulus results from both crosshead displacement and OT were found to have a slight inverse relation between loading rate and Young's modulus, in agreement with Linul et al. [37].

Limitations and Sources of Error

Using the OT methodology some small errors will result from out of plane movement of the specimen due to Poisson's ratio effects. As a result, markers will appear larger, increasing measured strain. However, for the experimental setup within this paper, this error will be small (less than 1% [28]). Markers of each specimen were drawn on by hand and therefore not in identical positions for each specimen. This is primarily an issue for Poisson's ratio calculation as endpoint effects will be dependent on their proximity to the ends due to Saint-Venant's effects [38].

Errors also arise from the imaging itself. Lens distortion has not been taken into account, mainly because specimen displacement during the test was negligible compared to the specimen size. Lighting variation and varying air index distortions can sometimes cause some errors, even though they are generally small when the testing conditions are well controlled [39]. As stated previously, the main error associated with out-of-plane movements is accounted for by the back-to-back camera set-up.

The OT methodology results were supported by good agreement with spatially rich DVC results. Some error in the DVC calculation will result from noise present in scans being falsely interpreted as strain. However initial analysis performed on repeat (unloaded) scans showed a positive mean strain bias of $\sim 1.2 \times 10^{-5}$ and standard deviation of strain of 1.4×10^{-4}. The sparse closed pore structure of the foam required a relatively high subvolume size as sufficient material is required for accurate correlation. This meant that high strain gradients could not be measured; while they may exist within the microstructure (pore connections), no sharp discontinuity was observed over the bulk material.

Conclusions

This study demonstrates that methods of measuring displacement data on cellular foams must be carefully considered, as artefacts can lead to significant errors. In particular, strains derived from cross-head displacement should not be used without compliance correction as they lead to gross underestimation of the Young's modulus. OT was found to be an inexpensive and highly accurate measurement option (when tested against VFM/DVC), which avoids measurement artefacts and setup issues associated with the use of multiple extensometers. The accuracy of Poisson's ratio and Young's modulus could be further improved by using an FE-derived correction factor taking into account the fact that the strains are not uniform through the thickness (for Young's modulus and Poisson's ratio) and the fact that the end constraints block Poisson's effect (for Poisson's ratio). This correction depends on the specimen size and nominal Poisson's ratio as shown in appendix Table 5.

The present study sought to develop a methodology that could evaluate the effect of experimental artefacts associated with uniaxial compression, through non-contact measurement and FE-based correction. The full-field DVC strain measurement technique coupled with VFM was found to account for these artefacts. However, the OT method could also identify heterogeneous responses during testing, which could be aggregated to produce an overall response at considerably reduced expense and complexity. The presented procedure could lead to a standard method to simply and accurately measure stiffness properties of rigid foam blocks, taking full advantage of the availability of inexpensive CDD cameras and image processing software.

Acknowledgments The authors wish to extend thanks to Dr. Mark Mavrogordato from the μVIS Computed Tomography Centre at the University of Southampton (Engineering and Physical Sciences Research Council grant EP-H01506X) for performing the scans presented in this work.

Mr. A. Marter would like to acknowledge the *Engineering and Physical Sciences Research Council,* who funded Alex's CASE Conversion studentship via a Doctoral Training Grant award ref. EP/L505067/1 and DePuy Synthes. Prof. F. Pierron acknowledges support from the Wolfson Foundation through a Royal Society Wolfson Research Merit Award. Dr. A. Dickinson acknowledges Research Fellowship funding from the Royal Academy of Engineering (Grant RF/130). These funding bodies had no direct involvement in conducting the study or the decision to submit it for publication.

Compliance with Ethical Standards

Conflict of Interest The Author(s) declare(s) that there is no conflict of interest.

References

1. Thirumal M, Khastgir D, Singha NK, Manjunath BS, Naik YP (2008) Effect of foam density on the properties of water blown rigid polyurethane foam. J Appl Polym Sci 108:1810–1817
2. Maji A, Schreyer H, Donald S, Zuo Q, Satpathi D (1995) Mechanical properties of polyurethane-foam impact limiters. J Eng Mech 121:528–540
3. Jin H, Lu W-Y, Scheffel S, Hinnerichs TD, Neilsen MK (2007) Full-field characterization of mechanical behavior of polyurethane foams. Int J Solids Struct 44:6930–6944
4. Jackovich D, O'toole B, Hawkins MC, Sapochak L (2005) Temperature and mold size effects on physical and mechanical properties of a polyurethane foam. J Cell Plast 41:153–168
5. Szivek J, Thomas M, Benjamin J (1993) Technical note. Characterization of a synthetic foam as a model for human cancellous bone. J Appl Biomater 4:269–272
6. Szivek JA, Thompson JD, Benjamin JB (1995) Characterization of three formulations of a synthetic foam as models for a range of human cancellous bone types. J Appl Biomater 6:125–128
7. Patel PS, Shepherd DE, Hukins DW (2008) Compressive properties of commercially available polyurethane foams as mechanical models for osteoporotic human cancellous bone. BMC Musculoskelet Disord 9:137
8. Calvert KL, Trumble KP, Webster TJ, Kirkpatrick LA (2010) Characterization of commercial rigid polyurethane foams used as bone analogs for implant testing. J Mater Sci Mater Med 21:1453–1461
9. Thompson MS, McCarthy ID, Lidgren L, Ryd L (2003) Compressive and shear properties of commercially available polyurethane foams. J Biomech Eng 125:732–734
10. Palissery V, Taylor M, Browne M (2004) Fatigue characterization of a polymer foam to use as a cancellous bone analog material in the assessment of orthopaedic devices. J Mater Sci Mater Med 15:61–67
11. Gillard F, Boardman R, Mavrogordato M, Hollis D, Sinclair I, Pierron F, Browne M (2014) The application of digital volume correlation (dvc) to study the microstructural behaviour of trabecular bone during compression. J Mech Behav Biomed Mater 29:480–499
12. Keaveny TM, Pinilla TP, Crawford RP, Kopperdahl DL, Lou A (1997) Systematic and random errors in compression testing of trabecular bone. J Orthop Res 15:101–110
13. Hamilton AR, Thomsen OT, Madaleno LAO, Jensen LR, Rauhe JCM, Pyrz R (2013) Evaluation of the anisotropic mechanical properties of reinforced polyurethane foams. Compos Sci Technol 87:210–217
14. Crammond G, Boyd S, Dulieu-Barton J (2013) Speckle pattern quality assessment for digital image correlation. Opt Lasers Eng 51:1368–1378
15. Villegas DF, Maes JA, Magee SD, TLH D (2007) Failure properties and strain distribution analysis of meniscal attachments. J Biomech 40:2655–2662
16. Nguyen M-T, Allain J-M, Gharbi H, Desceliers C, Soize C (2016) Experimental multiscale measurements for the mechanical identification of a cortical bone by digital image correlation. J Mech Behav Biomed Mater 63:125–133
17. Dickinson AS, Taylor AC, Browne M (2012) The influence of acetabular cup material on pelvis cortex surface strains, measured using digital image correlation. J Biomech 45:719–723
18. Srinivasan P, Miller MA, Verdonschot N, Mann KA, Janssen D (2016) Experimental and computational micromechanics at the tibial cement-trabeculae interface. J Biomech 49:1641–1648
19. Tozzi G, Danesi V, Palanca M, Cristofolini L (2016) Elastic full-field strain analysis and microdamage progression in the vertebral body from digital volume correlation. Strain 52:446–455
20. Madi K, Tozzi G, Zhang QH, Tong J, Cossey A, Au A, Hollis D, Hild F (2013) Computation of full-field displacements in a scaffold implant using digital volume correlation and finite element analysis. Med Eng Phys 35:1298–1312
21. Sukjamsri C, Geraldes DM, Gregory T, Ahmed F, Hollis D, Schenk S, Amis A, Emery R, Hansen U (2015) Digital volume correlation and micro-ct: An in-vitro technique for measuring full-field interface micromotion around polyethylene implants. J Biomech 48:3447–3454
22. Bay BK, Smith TS, Fyhrie DP, Saad M (1999) Digital volume correlation: Three-dimensional strain mapping using x-ray tomography. Exp Mech 39:217–226
23. Keaveny TM, Morgan EF, Niebur GL, Yeh OC (2001) Biomechanics of trabecular bone. Annu Rev Biomed Eng 3:307–333
24. Harrigan TP, Jasty M, Mann RW, Harris WH (1988) Limitations of the continuum assumption in cancellous bone. J Biomech 21:269–275
25. Moulart R, Pierron F, Hallett SR, Wisnom MR (2011) Full-field strain measurement and identification of composites moduli at high strain rate with the virtual fields method. Exp Mech 51:509–536
26. Kim JH, Pierron F, Wisnom MR, Syed-Muhamad K (2007) Identification of the local stiffness reduction of a damaged composite plate using the virtual fields method. Compos A: Appl Sci Manuf 38:2065–2075
27. Grédiac M, Pierron F, Avril S, Toussaint E (2006) The virtual fields method for extracting constitutive parameters from full-field measurements: A review. Strain 42:233–253
28. Pierron F (2010) Identification of poisson's ratios of standard and auxetic low-density polymeric foams from full-field measurements. J Strain Anal Eng Des 45:233–253
29. Tattoli F, Pierron F, Rotinat R, Casavola C, Pappalettere C (2010) Full-field strain measurement on titanium welds and local elasto-plastic identification with the virtual fields method. International Conference on Advances in Materials and Processing Technologies, Pts One and Two 1315:860–865

30. Avril S, Pierron F, Sutton MA, Yan JH (2008) Identification of elasto-visco-plastic parameters and characterization of luders behavior using digital image correlation and the virtual fields method. Mech Mater 40:729–742
31. Dym CL, Shames IH (1973) Solid mechanics. Springer, New York
32. Pierron F, Grédiac M (2012) The virtual fields method: Extracting constitutive mechanical parameters from full-field deformation measurements. Springer Science & Business Media, New York
33. Pannier Y, Avril S, Rotinat R, Pierron F (2006) Identification of elasto-plastic constitutive parameters from statically undetermined tests using the virtual fields method. Exp Mech 46: 735–755
34. Moulart R, Avril S, Pierron F (2006) Identification of the through-thickness rigidities of a thick laminated composite tube. Compos A: Appl Sci Manuf 37:326–336
35. Pierron F (1998) Saint-venant effects in the iosipescu specimen. J Compos Mater 32:1986–2015
36. Pierron F, Cerisier F, Grediac M (2000) A numerical and experimental study of woven composite pin-joints. J Compos Mater 34: 1028–1054
37. Linul E, Marsavina L, Voiconi T, Sadowski T (2013) Study of factors influencing the mechanical properties of polyurethane foams under dynamic compression. Journal of Physics, Conference Series, p 012002
38. de Saint-Venant M (1856) Mémoire sur la torsion des prismes: Avec des considérations sur leur flexion ainsi que sur l'équilibre intérieur des solides élastiques en général: Et des formules pratiques pour le calcul de leur résistance à divers efforts s' exerçant simultanément. Imprimerie Nationale, Paris
39. Badaloni M, Rossi M, Chiappini G, Lava P, Debruyne D (2015) Impact of experimental uncertainties on the identification of mechanical material properties using dic. Exp Mech 55:1411–1426